Raman Microscopic Line Imaging

Gary Hastings and R. Brian Dyer*

Los Alamos National Laboratory

Chemical Science and Bioscience Division

CST-4, MS J586

Los Alamos, NM 87545

Index Headings: Raman Microscopy, Hyperspectral Imaging, Line Imaging

Abstract

A hyperspectral Raman imaging microscope has recently been developed for studies in many areas. The microscope can be used in either a point focusing mode, where spectra are collected at each point in a sample, or in a line imaging mode, where spectra are obtained simultaneously at each point on a line across a sample. The system can also be used for dual fluorescence/Raman measurements and can be operated in a psuedo macroscopic mode. Some capabilities of the system are highlighted and discussed in the context of images and spectra obtained using various materials, including single red blood cells. Some recent applications are also outlined and discussed.

*Corresponding Author

Abbreviations: RBC, red blood cell; SERS, surface enhanced Raman spectroscopy; CCD, charge coupled device

Introduction

In the last several years microscopic Raman techniques have matured dramatically. Advances in detector as well as filter technology has allowed the construction of robust, compact, high throughput micro-Raman systems. These systems have found applications in diverse areas[1] from ceramics[2,3] and polymers[4-7] to medicine[8,9] and pigment analysis of fine art[10,11].

Most of the applications detailed to date use a laser beam focused to a small spot on the sample (point illumination). The scattered light is collected and dispersed, then detected using either a linear multi-element array or a CCD camera. In this way a highly resolved Raman spectrum can be obtained and, with the use of confocal optics, spectra can be obtained from very small volumes of sample (<1 μm^3). By moving the sample, a 2D grid of spectra can be obtained. Raman spectral images are generated by plotting the intensity of the Raman band or bands of interest at each sample position.

The information that can be obtained using a confocal, micro-Raman system is 4 dimensional (3 spatial and one spectral). Almost all modern micro-Raman systems utilize sensitive CCD cameras so that 2 dimensions of the available 4 dimensional information can be collected simultaneously. Some type of scanning is required to collect data in the remaining dimensions. The difference between the available micro-Raman systems is usually associated with the dimensions which are scanned.

Another approach to Raman imaging has been developed which probes two spatial dimensions at a single frequency. In this approach the sample is illuminated globally but usually not uniformly. Some sort of filter is used to select a single frequency and a 2D detector is used to form an image at this frequency. In the past, spectral resolution has somewhat limited the utility of this technique, however, recent advances in tunable, liquid crystal filter technology look promising[12]. It is not possible to use this direct Raman imaging approach in a confocal mode so the data that can be obtained is essentially only three dimensional, with the possibility that out of focus scattered light

may obscure or blur the Raman images. In the near future, however, we expect it will be possible to generate confocal images without the confocal aperture, using newly developed algorithms that operate on stacks of "blurred" images taken at different depth positions (see Shaw[13] and Holmes et al.[14], and references therein). Another possibility may be to generate a "virtual" aperture using a CCD camera[15].

The point focusing approach outlined above, when operated in a confocal geometry, can give well resolved 4D information. However, this approach does not utilize the 2D capabilities of a CCD camera. As a result it is an extremely, often impractically, time consuming approach. A superior approach is to use either an optical scanner or a cylindrical lens to image the laser beam to a line on the sample. This line can then be imaged onto the entrance slit of a stigmatic, imaging spectrograph, attached to a CCD camera. The 2D images obtained contain one spatial and one spectral dimension. To obtain 2D spatial information the sample is moved in one dimension perpendicular to the length of the scanned laser line (line mapping). There are at least two additional advantages of the line scanning approach: Firstly the spectrograph slit acts as a spatial filter, providing some confocal capability. Secondly, heating effects, resulting in sample damage, are reduced, compared to point illumination. Imaging the scanned laser line onto the slits of a spectrograph maximizes the illuminated area. For a given average incident power the amount of scattered light will be the same in both point and line illumination modes, but in line illumination mode the average power can be increased without optical damage because the power density is substantially decreased. Ivanda and Furic[16] found for their experimental setup that for the same excitation power density in point and line illumination, line illumination gave a factor of 18 improvement (depending on the length of the scanned laser line) in signal to noise ratio over point illumination.

Several authors have considered line imaging: Ivanda and Furic[16] analyzed a line focusing system, which utilized a cylindrical lens. Their instrumentation did not,

however, preserve spatial information along the line. Drumm and Morris[17] used a cylindrical lens for line focusing while Bowden et al[18] used a scanning lens. Viers et al[19, 20] also used a cylindrical lens, with an imaging photomultiplier tube to obtain spatially resolved spectra.

Of the two approaches to line imaging (cylindrical lens or laser scanning) laser scanning is the best choice for two reasons. Firstly, when using a cylindrical lens to generate a line, the intensity distribution along the line will be asymmetric or Gaussian. Secondly, if scanners are used it is possible to make the system truly confocal[21, 22].

We report here on the development of a line imaging Raman microscope that can produce high resolution, spatially resolved spectra. We also describe techniques we have developed for producing two dimensional, spatially resolved, Raman (spectral) images.

Materials and Methods

Figure 1 shows a schematic of the line imaging Raman microscope used here. The system is built around a Zeiss Axiovert TV microscope. Unless stated, the 514.5 nm line from a Spectra Physics 2045 argon ion laser was used for excitation. The excitation intensity at the sample was controlled using neutral density filters. The laser beam was scanned prior to entering the microscope using a Cambridge Technology optical scanner controlled by a Dana Exact, model 506 sweep/function generator. For point focusing the signal generator is simply switched off. The signal generator allows control of the line scan frequency and amplitude. The length of the line at the sample depends on the objective lens. Two objective lenses were used in the work described here: Either a Zeiss, Achroplan, infinity corrected, 63X dry objective lens (NA=0.95) or a Zeiss LD epiplan, infinity corrected, 20X dry objective lens (NA=0.4). The focused laser line is ~ 130 or 40 μm in length when the 20X or the 63X objective is used, respectively. In the figure legends we will simply refer to the objectives as the 63X or 20X objective.

The scattered light from the scanned excitation laser line is collected by the objective lens (180 degree backscatter geometry). A tube lens inside the microscope forms a primary image (which is located just outside the microscope) and then a second lens (L1 in fig 1) further magnifies and images the scanned line onto the entrance slit of a Kaiser HoloSpec f/2.2 imaging spectrograph. The total magnification depends on the focal length of lens L1. An external holographic notch filter (Kaiser supernotch plus) is used to reject the laser line. For all line imaging a 50 μm slit was used (for some of the spectra collected in point focus mode a 25 μm slit was used), resulting in a spectral resolution of ~5.7 cm^{-1}. Spectral calibration is performed using either standard lamp lines or the Raman bands of toluene.

Detection is accomplished with a Photometrics C210 CCD camera attached to the holoSpec (for some point focus applications we also used a 0.25 m Acton spectrograph). The camera has a prime grade 512x512 chip with very few "bad" pixels. The vertical dimension (parallel to the slit) on the CCD camera contains spatial information while the horizontal dimension contains spectral information.

One disadvantage of the holospec is that it has a fixed grating which is optimized only for a specific excitation wavelength (as are the coated optics). So for different excitation wavelengths a different spectrograph is required. Our spectrograph can image the 50-2480 cm^{-1} spectral region with 514.5 nm excitation (low frequency Stokes grating), assuming a 25 mm detector width. Our CCD camera is ~ 12 mm wide so to cover the full spectral range the CCD camera was translated perpendicular to the holospec optical axis.

To obtain 2D spatial information the sample is translated in the direction perpendicular to the laser line using a Cell Robotics translation stage, which is accurate to 0.1 μm. A PowerMac 7100/80 computer is used to control data acquisition and all (serially interfaced) peripheral devices. In point focus mode the CCD is binned and a 3-point median filter is applied to the spectra (this effectively eliminates cosmic ray

spikes) before presentation. In the line focusing work described here the data obtained consist of stacks of line images. All spectra and image stacks are collected and processed in an automated fashion using custom software generated in IPLab.

In point illumination mode, the image of the point (actually the point is a diffraction limited spot (Airy disk) of diameter 0.66 μm for 514.5 nm excitation) on the CCD is a few pixels wide but spans the full length of the CCD (spectral dimension). When collecting spectra we can simply bin the CCD but in many cases, in order to reduce readout noise, to speed up processing time and to increase the confocal capabilities of the system[15], we collect and bin only the narrow strip of pixels that contain the spectral information.

Slightly different set-ups were used for point and line focusing although this was not strictly necessary. For point focusing a 50 mm achromatic lens was used to focus the Raman light to a point at the slit. For line focusing the focal length of the achromatic field lens (L1) could be varied depending on the desired magnification. In most circumstances we chose lens L1 such that the length of a ~0.5 μm spot would be imaged onto 2-4 pixels (46-92 μm in our CCD camera).

Results

Point Focusing Figure 2 shows spectra obtained from (a) a 1 μm polystyrene bead and (b) a crystal of ammonium sulfate. From (a) it is clear that we can obtain relatively intense spectra from sample volumes of the order of 1 μm^3. For many crystals it is relatively simple to obtain Raman spectra at the microscopic level. For ammonium sulfate, in the 800 to 1600 cm^{-1} region, there is only one prominent Raman band, near 1000 cm^{-1}. By collecting spectra at each point on a 10x10 regular square grid (10 μm increments) and then selecting the ~1000 cm^{-1} band (integrating over the whole area of the band) in each spectrum we were able to construct a ~1000 cm^{-1} Raman image of the crystal and this is shown in figure 3. The image in (C) is of low spatial resolution. If images with high spatial resolution are required, the point illumination technique is likely

to be prohibitively time consuming. To increase data collection rates (by using the full capacity of the CCD) we developed a laser scanning system.

Line Scanning In any laser scanning system it is important to be able to move quickly and easily between point and line scanning modes. In our system this can simply be done by switching off the optical scanner. Figure 4 shows the line image obtained from a flat sheet of polystyrene. Under the conditions of this particular experiment, less than half the total area of the CCD is being used. As mentioned, this can be changed simply by changing the lens L1 in figure 1, however, the image would contain redundant information because the image of a diffraction limited resolution element (~0.66 μm) would span several pixels. In figure 4 it is also clear that the lines are somewhat curved. This curvature is intrinsic to all stigmatic imaging spectrographs but is more pronounced for short focal length systems, such as the holospec. For the central 3 mm of the image on the CCD the deviation is less than one pixel (~23 μm) so no correction is required. For images covering larger areas some correction is required. The image curvature can be well characterized and we are currently in the process of generating pixel shifting algorithms to compensate for the deviation.

In figure 4, and all the line images to be presented here, the horizontal dimension is the spectral dimension. So, by adding or averaging columns of pixels (binning the image pixels vertically) spectra can be obtained. If the columns in the image in figure 4 are summed, a spectrum identical to that shown in figure 2(A) is obtained. By switching off the scanner the lines in figure 4 collapse to a point (data not shown).

To demonstrate the spatial resolution of the line imaging system we have performed measurements using polystyrene beads with a diameter of ~4.3 μm. Figure 5 shows a line image obtained for a single bead. Raman scattered photons are detected only from regions where the laser line is in contact with the polystyrene. Since the beads have a known diameter it is possible to calibrate the CCD pixels in the spatial

dimension. By selecting the rectangular region around the ~ 1000 cm^{-1} band (shown in figure 5) and then summing the rows of pixels (horizontal binning) in the selected region, the intensity distribution in figure 6 is obtained. The half width of the intensity distribution function is ~17 pixels. Since the bead has a diameter of 4.3 μm, ~4 pixels corresponds to 1μm. The 10 to 90% rise on either side of the intensity distribution function is ~4 pixels, or ~1 μm (see inset in figure 6). We also find that the intensity distribution in figure 6 is identical to that which can be obtained for the bead at any other position along the scanned laser line.

To obtain 2D spatial information it is necessary to translate the sample in a direction perpendicular to the scanned laser beam, and collect line images (as in figure 5) at each sample position. 2D, spatially resolved images can then be reconstructed from such a stack of line images. Figure 7 shows an image of a 4.3 μm polystyrene bead, constructed using the ~ 1000 cm^{-1} polystyrene band. For this image the polystyrene bead was translated through the scanned excitation laser line, in 1 μm increments. For each image in the stack of images, a rectangular region around the 1000 cm^{-1} band was selected. The pixel width of the rectangle was chosen so that it corresponded to ~1 μm (the same as the sample translation increments). So both spatial dimensions in figure 7 are scaled similarly. These rectangular strips were pasted in sequence into a new image and figure 7 is an example of one of many possible spectral image reconstruction's. These image reconstruction procedures were performed in an automated fashion using custom software.

To show that we have some confocal capability we also collected a set of line images for a 4.3 μm bead (located centrally on the scanned laser line) as it was translated in the axial direction, along the optical axis of the microscope (normally denoted as the z-axis). Images identical to that in figure 7 were obtained (data not shown). By again selecting the 1000 cm^{-1} band in each image and binning the pixels horizontally (as in figure 5) we obtain spatially resolved intensity distributions as a

function of the depth parameter, z. These intensity distributions are shown in figure 8. Clearly, by changing the sample depth by 1-2 μm we can readily observe a significant decrease in the intensity of the 1000 cm^{-1} band across the bead, indicating that the system has some confocal capabilities. The Raman intensity does not drop to zero until the bead is positioned ~ 7 μm, from where the scanned laser line intersects the center of the bead. Taking into account the ~2.15 μm radius of the bead and the ~0.5 μm confocal parameter associated with the scanned laser line, it appears that we can detect some Raman light at a distance of ~4 μm from the focal position of the scanned laser line, although the intensity is much diminished. If we are able to compare intensity distributions of Raman bands then it would appear that we are able to distinguish sample depth displacements of at least 1 μm.

Species Distribution in Samples Line imaging is ideally suited to investigate directly the distribution of species in a sample. For example two such projects we have underway are to investigate the distribution of uranium compounds in soil samples and the distribution of compounds in polymers (see below). As an example of the utility of this technique we have used line imaging to image a mixture of crystals of boric acid and ammonium sulfate.

For ammonium sulfate, in the 800 to 1600 cm^{-1} region, there is only one prominent Raman band, near 1000 cm^{-1} (see figure 2B). For boric acid, in the same spectral region, a single Raman band, at ~880 cm^{-1} dominates the spectrum[23] (data not shown). So we can use the ~880 cm^{-1} band of boric acid and the ~1000 cm^{-1} band of ammonium sulfate to distinguish between the two species. Figure 9 shows a bright field image of an irregularly shaped crystal mix of ammonium sulfate and boric acid. Using a 20X objective the scanned laser line (represented as a solid black line in figure 9) spans the length of the crystals. The crystal mix was translated through the scanned laser beam in 3 μm increments. At each position a line image was collected. Forty eight line images were collected in all. Figure 10 shows an example of a line image collected

when the scanned laser line is at the position shown by the black line in figure 9. The 880 cm^{-1} and 1000 cm^{-1} bands associated with the different types of crystals are obvious. An image reconstruction of the ~ 1000 cm^{-1} ammonium sulfate band is shown in figure 11, and the 880 cm^{-1} band of boric acid in figure 12. The two images taken together are clearly complementary and accurately describe the brightfield image in figure 9. Although not obvious from the bright field image in figure 9, the Raman image in figure 11 clearly indicates that the top piece of the crystal mix is ammonium sulfate and so is some portion at the bottom right of the mix. The intensity differences in the two pieces of ammonium sulfate crystal may be due to different depths of the two pieces. To fully resolve this issue we would need to collect data in the axial dimension (the z-axis).

Application to Living Cells: Red Blood Cells As an example of the line imaging technique applied to living cells we have performed measurements on red blood cells (RBC's). RBC's are biconcave disks with a diameter of ~ 8 μm[24]. Much of the volume of RBC's is occupied by the oxygen storage and transport protein, hemoglobin, hence it is likely that any Raman spectra we obtain will be due to hemoglobin. In addition, we expect significant resonance enhancement of hemoglobin Raman bands because 514.5 nm is coincident with the β absorption band of the heme[25].

Figure 13 shows the Raman spectrum obtained following 514.5 nm excitation of a single RBC. The spectrum is clearly reminiscent of hemoglobin[25]. The band near 1365 cm^{-1} depends on the oxygenation state of the hemoglobin and is typically 1355 cm^{-1} for the deoxy form, 1379 cm^{-1} for the oxy form of hemoglobin. We have noted several factors that can influence the shape of the cell with concomitant changes in both the intensity and position of some of the Raman bands. This is beyond the scope of the present work, the purpose of which is simply to show the utility of the line scanning Raman system.

Figure 14 shows a line image obtained when the scanned laser beam traverses the middle of a RBC. Clearly there is a large decrease in intensity in the middle of the cell, consistent with it's biconcave shape. The thickness of RBC's vary from ~ 1.5 μm near the middle up to ~1.8 μm near the periphery[24]. This indicates that we are able to observe sub micron level changes in living cells. By binning the pixels in figure 14 vertically we obtain a spectrum identical to that shown in figure 13 and by binning the pixels in figure 14 horizontally we can gain an impression of the shape of the cell. Figure 15 shows the results of such horizontal binning. Clearly the Raman bands of hemoglobin can be used to form images of single cells. The shape of RBC's depend on the experimental conditions (and on various disease states) so it is possible to track not only molecular decomposition (by monitoring changes in the Raman spectra) but also where this decomposition occurs in the cell. In some cases we were unable to observe decreased intensity in the middle of the cell (as is shown here). Instead we observe almost uniform Raman intensity across the cell, indicating the cells are more spherical in shape.

Discussion

The advantages of Raman imaging over other spectral imaging techniques such as fluorescence, are obvious, although much greater sensitivity is required using the Raman approach. In fluorescence microscopy, usually molecular tags or labels are used which attach to specific molecular components. The fluorescence from these tags is then used to image the molecular component. The process of tagging is generally complex and time consuming. It is often the case that these tags can damage or perturb the material they are supposed to report on, and this is especially true for biological material. In addition, the broadband nature of the fluorescence limits the number of components that can be imaged at any one time. In contrast, no tags are required for Raman imaging in principle (although it is certainly feasible and Raman

tags have been used successfully recently[26]) and hence any potentially perturbative effects of the tags are removed. In addition, the vibrational technique is more selective of the type of molecules probed and will detect structural changes to which fluorescence spectra are insensitive. With Raman microscopy it is possible to also selectively image different components by resonance enhancement of specific components. In the study of single cells for example, the molecular species that will dominate the image (DNA, cytochromes, carotenoids, etc.) can be selected simply by varying the frequency of laser excitation. The high spatial resolution attainable using Raman microscopy (demonstrated here) should enable the study of subcellular components. With heme proteins, the use of certain visible excitation wavelengths will resonantly enhance scattering making the study of these proteins particularly attractive. Imaging of heme proteins in single cells is underway and recently studies on myeloperoxidase and cytochrome b have been presented[27].

Measurements on RBC's, such as those described here, are likely to be of great value in studies related to blood storage. As stored blood ages, the hemoglobin in the cells undergoes chemical changes and decomposition. The details of these changes are not known precisely but it is certain that these changes will be accompanied by specific changes in the Raman spectra of the cellular hemoglobin. The use of Raman microscopy is therefore likely to be a useful probe of these cellular modifications.

In addition to the obvious advantages of Raman spectroscopy, modern computer algorithms (which can combine several tens or even hundreds or thousands of spectral images to produce a hyperspectral image) and image enhancement techniques applied to spectral microscopy will likely produce hyperspectral images that are far superior to that of images at single frequencies. Figures 7, 11, 12 show three, single frequency Raman images which represent only a tiny fraction of the total data collected. There is a huge amount of detailed information in the image stacks that has not been used in any constructive way, mainly because of the lack algorithms that can appropriately

manipulate the hyperspectral data. We have obtained images as in figure 7 for all the polystyrene bands. The signal to noise ratio in each image is different, so simply adding the images together generally does not produce a composite image that is superior (both numerically and aesthetically) to all of the single frequency Raman images[30]. More complex algorithms are required to utilize the information content inherent in large hyperspectral image stacks. Hyperspectral image analysis is still in its infancy but with the launch of various airborne spectral imagers such as AVIRIS (Airborne Visible/Infrared Imaging spectrometer) there has been a flurry of activity in the field[28-31]. Important areas of research are 1/ the development of data reduction algorithms that can reduce or compress the huge volume of hyperspectral data without loss of critical information[28, 29] and 2/ the development of image fusion algorithms that can combine several spectral images into a composite image that contains more detail and less noise than any single spectral image on its own[30, 31]. Activities in the area of hyperspectral image analysis is likely to increase dramatically in the near future, partly because the next generation of airborne spectral imagers have been developed (for example, the high spectral imager (HSI)[32] is expected to be launched soon[33]) and partly because of the wide interest in, and applicability of spectral microscopies.

There are several areas in which Raman microscopic line imaging may be an extremely useful analytical tool. Here we describe a few of the studies that are currently in progress in our lab.

One project we are just embarking on is in the study of etched or patterned self assembled monolayers. Molecular monolayers and thin films are of interest for many applications, including non-linear optical materials, biological sensors, protective layers and protein films. Lack of techniques for accurately monitoring the growth and characteristics of organic thin films has hindered the development and application of this technology but micro Raman imaging may be a useful diagnostic tool for thin film characterization[34, 35]. We expect the line imaging approach developed here to be an

extremely powerful diagnostic tool for the study and characterization of microscopically patterned monolayers. In such monolayer studies the number of Raman photons is extremely low, so the development of this field is intimately dependent on the generation of surfaces with suitable characteristics for surface enhanced Raman spectroscopy (SERS). In fact, azobenzene monolayers have recently been used specifically for the characterization of differently prepared SERS active surfaces[34].

Uranium Complexes in Soil: A significant problem facing the US DOE is contamination of soils at various production and testing facilities. Remediation of contaminated sites depends on speciation information. Information of the oxidation state and chemical form of contaminants is a necessary precursor for the utilization of remediation technologies. Raman microspectroscopy can be of great value in this area. Not only for species identification but also for monitoring decontamination technologies, and recently we have studied some uranium contaminated soil samples.

Under bright field illumination we have found that it is almost impossible to visualize uranium complexes in contaminated soil samples. This is not the case using fluorescence techniques, however. Many actinide complexes exhibit strong fluorescence and can therefore be visualized directly. The Zeiss axiovert microscope is ideally suited for combined Raman/fluorescence studies. For fluorescence studies we illuminated (with light from the condenser lamp) the soil samples from one side using the normal condenser optics in combination with an appropriate excitation filter. This allowed visualization of the various actinide complexes in the sample which could then be translated to coincide with the laser excitation beam coming from the opposite direction. In this way we have been able to differentiate various compounds in soil samples. Again we expect the line imaging techniques developed here to be extremely useful for mapping species distribution in these samples.

Acknowledgments

We would like to thank Lauren Peterson of the Environmental Research Institute of Michigan (ERIM) for many useful discussions.

References

1 P. J. Treado and M. D. Morris, in *Microscopic and Spectroscopic Imaging of the Chemical State,* M. D. Morris, Ed. (Marcel Dekker, New York, 1993), p. 71.

2 I. Siny, S. Sen, R. S. Kitayer, S. Bhattacharya and D. C. Agrawal in *Proceedings of the XV th International Conference on Raman Spectroscopy*, S. A. Asher and P. B. Stein, Eds. (John Wiley and Sons, New York, 1996), p. 1160.

3 J. D. Belnap, J-F. Tsai and D. K. Shetty, J. Mater. Res. **9**, 3183 (1994)

4 A. Garton, D. N. Batchelder and C. Cheng, Appl. Spectrosc. **47**, 922 (1993)

5 R. Tabaksblat, R. J. Meier and B. J. Kip, Appl. Spectrosc. **46**, 60 (1992)

6 N. Everall, K. Davis, H. Owen, M. J. Pelletier and J. Slater, Appl. Spectrosc. **50**, 388 (1996)

7 M. D. Schaeberle, C. G. Karakatsanis, C. L. Lau and P. J. Treado, Anal. Chem. **67**, 4316 (1995)

8 Y. Ozaki, Appl. Spectrosc. Revs. **24,** (3, 4), 259-312 (1988)

9 J. A. Centeno, Ishak, K. G., F. G. Mullick, W. A. Gahl and T. J. O'Leary, Appl. Spectrosc. **48**, 569-572 (1994)

10 R. Davey, D. J. Gardiner, B. W. Singer and M. Spokes, J. Raman Spectrosc. **25**, 53-57 (1994).

11 R. J. H. Clark, J. Molec. Struct. **347**, 417 (1995)

12 H. R. Morris, C. C. Hoyt, P. Miller, and P. J. Treado, Appl. Spectrosc. **50**, 805 (1996)

13 P. J. Shaw, in *Handbook of Biological Confocal Microscopy*, J. B. Pawley, Ed. (Plenum Press, New York, 1995) p. 373.

14 T. J. Holmes, S. Bhattacharyya, J. A. Cooper, D. Hanzel, V. Krishnamurthi, W-C. Lin, B. Roysam, D. H. Szarowski, and J. N. Turner, in *Handbook of Biological Confocal Microscopy*, J. B. Pawley, Ed. (Plenum Press, New York, 1995) p. 389.

15 K. P. J. Williams, G. D. Pitt, D. N. Batchelder and B. J. Kip, Appl. Spectrosc. **48**, 232 (1994)

16 M. Ivanda and K. Furic, Appl. Opt. **31**, 6371-6375 (1992)

17 C. A. Drumm and M. D. Morris, Appl. Spectrosc. **49**, 1331-1337 (1995)

18 M. Bowden, D. J. Gardiner, G. Rice and D. L. Gerrard, Appl. Spectrosc. **50**, 805-811 (1995)

19 D. K. Viers, G. M. Rosenblatt, R. H. Dauskardt and R. O. Ritchie, *Microbeam Analysis*, D. J. Newbury, Ed. 179 (1988)

20 D. K. Viers, J. W. Ager, E. T. Loucks and G. M. Rosenblatt, Appl. Opt. 29, 4969 (1990)

21 S. Sharonov, I. Nabiev, I. Chourpa, A. Feofanov, P. Valisa and M. Manfait, J. Raman Spectrosc., **25**, 699 (1994)

22 J. Barbillat, P. Dahmelincourt, M. Delhaye and E. Da Silva, J. Raman Spectrosc. **25**, 3-11, (1994).

23 G. J. Puppels, M. Grond and J. Greve, Appl. Spectrosc. **47**, 1256 (1993)

24 M. Bessis, *Corpuscles: Atlas of Red Blood Cell Shapes*, (Berlin, Springer-Verlag, 1974)

25 A. T. Tu, in *Raman Spectroscopy in Biology: Principles and Applications*, (Wiley, 1982) Ch. 12, p. 316

26 N. M. Sijtsema, J. J. Duindam, G. J. Puppels, C. Otto, and J. Greve, Appl. Spectrosc. **50**, 545 (1996)

27 N. M. Sijtsema, R. Ramanauskaite, G. M. J. Segers-Nolten, S. Arzhantsev, C. Otto and J. Greve, in *Proceedings of the XV th International Conference on*

Raman Spectroscopy, S. A. Asher and P. B. Stein, Eds. (John Wiley and Sons, New York, 1996), p. 1148.

28 J. C. Harsanyi, IEEE Transactions on Geoscience and Remote Sensing, **32**, 779 (1994)

29 S. Qian, A. B. Hollinger, D. Williams, D. Manak, Opt. Eng. **35**, 3242, (1996)

30 T. A. Wilson, S. K. Rogers, L. R. Myers, Opt. Eng. **34**, 3154 (1995)

31 G. P. Abousleman, E. Gifford and B. R. Hunt, Opt. Eng. **33**, 2562, (1994)

32 J. Marmo, Laser Focus World, p. 85, August (1996)

33 R. A. Mendonsa, Photonics Spectra, p. 18, February (1997)

34 T. Zhu, H. Z. Yu, J. Wang, Y. Q. Wang, S. M. Cai and Z. F. Liu, Chem. Phys. Letters **265**, 334 (1997)

35 X. M. Yang, D. A. Tryk, K. Hasimoto and A. Fujishima, Appl. Phys. Lett. **69**, 4020 (1996)

Figure Legends

Figure 1: Micro-Raman Setup. Abreviations: SS, scanning translation stage; Obj, objective lens; DR, dichroic reflector; Sh, shutter; HN, holographic notch filter; Sc, optical scanner; M1,2,3-mirrors; A primary image is formed near A. L1 is a field lens used to magnify (demagnify) the primary image from the microscope onto the slits of the holospec spectrograph. The distance from A to B is ~ 70 cm. The distance AC (or CB) and the focal length of L1, controls the magnification of the primary image.

Figure 2: Raman spectra, obtained in point illumination mode using 514.5 nm excitation. (A) Spectrum from a single 1 μm polystyrene bead. A 63X, dry objective lens was used. Excitation intensity, ~ 3.3 mW. Integration time, 6 seconds. Slits on holospec were set at 25 μm. (B) Spectrum from a single crystal of ammonium sulfate $(NH_4)_2SO_4$. A 20X dry objective lens was used. Excitation intensity, ~ 3.3 mW. Integration time, 6 seconds. Slits on holospec were set at 25 μm. The spectrum in (B) was devided by a factor of 2 and shifted for presentation.

Figure 3: Raman image of the ~1000 cm^{-1} band obtained using the same ammonium sulfate crystal as in (B). The crystal was translated in 10 μm increments on a regular grid and spectra were collected at each position. In each of the 100 spectra the ~1000 cm^{-1} band was selected and the integrated intensity measured. From these measurements a 2D Raman image of a crystal was constructed. An identical background image was also constructed at 1020 cm^{-1} and subtracted from the image obtained at ~1000 cm^{-1}. Experimental conditions as in (B).

Figure 4: Line image obtained from a flat polystyrene sheet. A 63X objective lens was used to image the 514.5 nm light to a sharp line at the sample. Excitation intensity was ~ 14 mW and an integration time of 30 seconds was used. The lines correspond to the Raman bands in figure 2(A). Slits on the holospec were set to 50μm.

Figure 5: Line image obtained from a single 4.3 μm polystyrene bead when the scanned laser line traverses the middle of the bead. Excitation intensity was ~ 14 mW and an integration time of 100 seconds was used.

Figure 6: Intensity distribution obtained by selecting a rectangular region around the ~ 1000 cm^{-1} line (shown in figure 5) and binning the selected pixels horizontally. Inset: blow up of the left edge of the curve. **Figure 7:** Two dimensional, spatially resolved image of the ~ 1000 cm^{-1} band obtained using a 4.3 μm bead. It was not necessary to construct and subtract a background image from the image in figure 7. Experimental conditions as for figure 5.

Figure 8: Line images of a 4.3 μm bead were obtained as the bead was translated along the z-axis. Again, by taking rectangular sections around the 1000 cm^{-1} line and binning the selected pixels horizontally, intensity distributions of the Raman band, as a function of z are obtained. Negative numbers in the figure indicate that the scanned laser line is focussed further into the bead. Experimental conditions as for figure 5.

Figure 9: Bright field image of a mix of boric acid (H_3BO_3) and ammonium sulfate ($(NH_4)_2SO_4$) crystals. The thick black line represents the orientation of the laser beam and the sample is translated perpendicular to this line.

Figure 10: Line image obtained from the crystal mix shown in figure 9. The position of the scanned excitation beam for this image is represented by the solid black line in figure 9. Forty eight line images were collected as the sample is translated through the scanned laser line, in 3 μm increments.

Figure 11: 2D, spatially resolved Raman image of the ~ 1000 cm^{-1} band of ammonium sulfate. The two spatial dimensions are approximately the same. Excitation intensity, ~15 mW. Integration time, 50 seconds. Slits on holospec, 50 μm.

Figure 12: 2D, spatially resolved Raman image of the ~ 880 cm^{-1} band of boric acid. The two spatial dimensions are approximately the same. Excitation intensity, ~15 mW. Integration time, 50 seconds. Slits on holospec, 50 μm.

Figure 13: Raman spectrum from a single red blood cell, obtained in point focus mode. A 63X objective was used. The spectrum in (A) is the average of 4 spectra which were collected using a 60 second integration time. Excitation is ~3.3 mW. A fitted function was used to correct the baseline. **Figure 14:** Line image obtained from a single red blood cell. Excitation intensity, ~14 mW. Integration time, 60 seconds.

Figure 15: Intensity distribution obtained by binning the pixels in figure 14 horizontally.

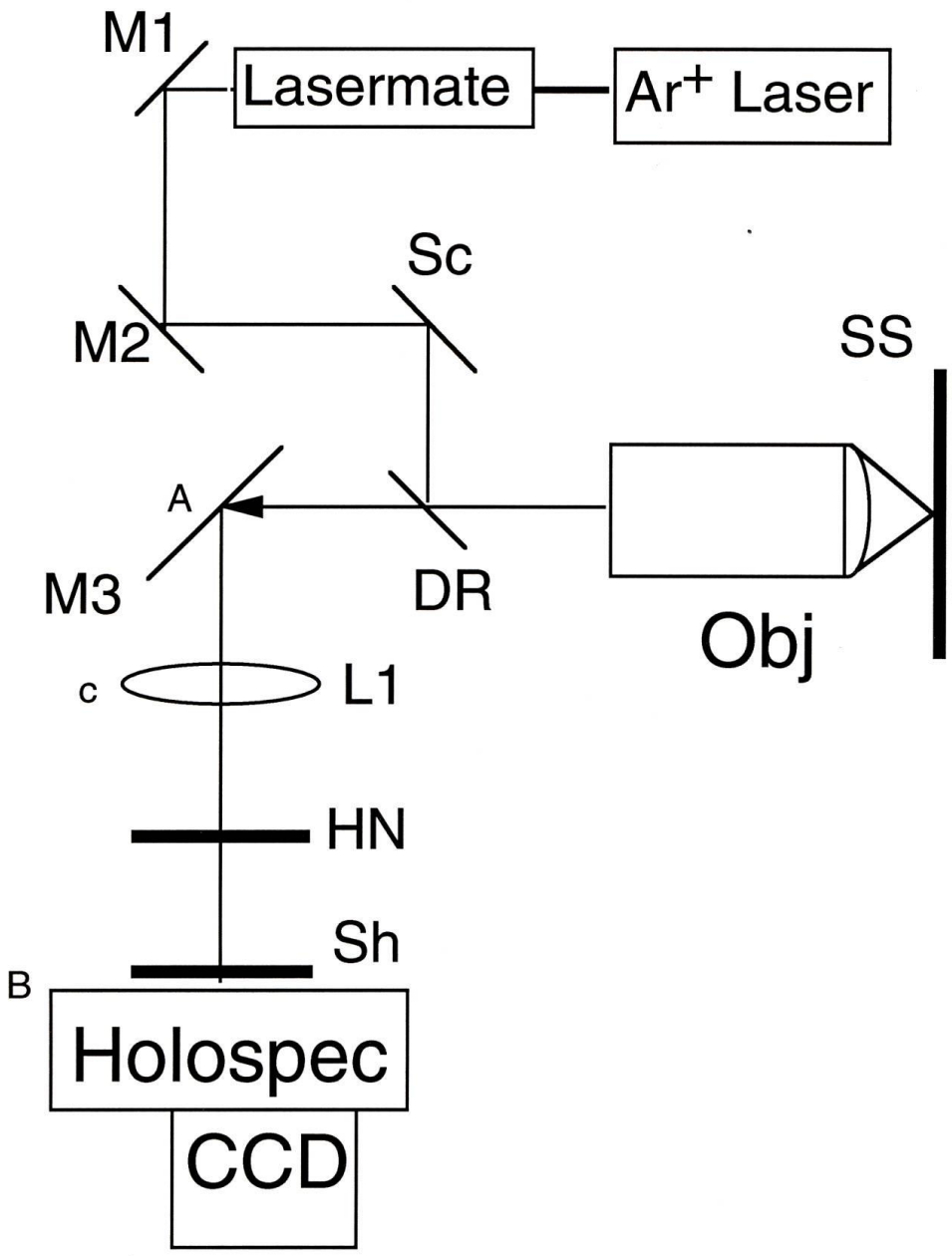

Figure 1, Hastings and Dyer

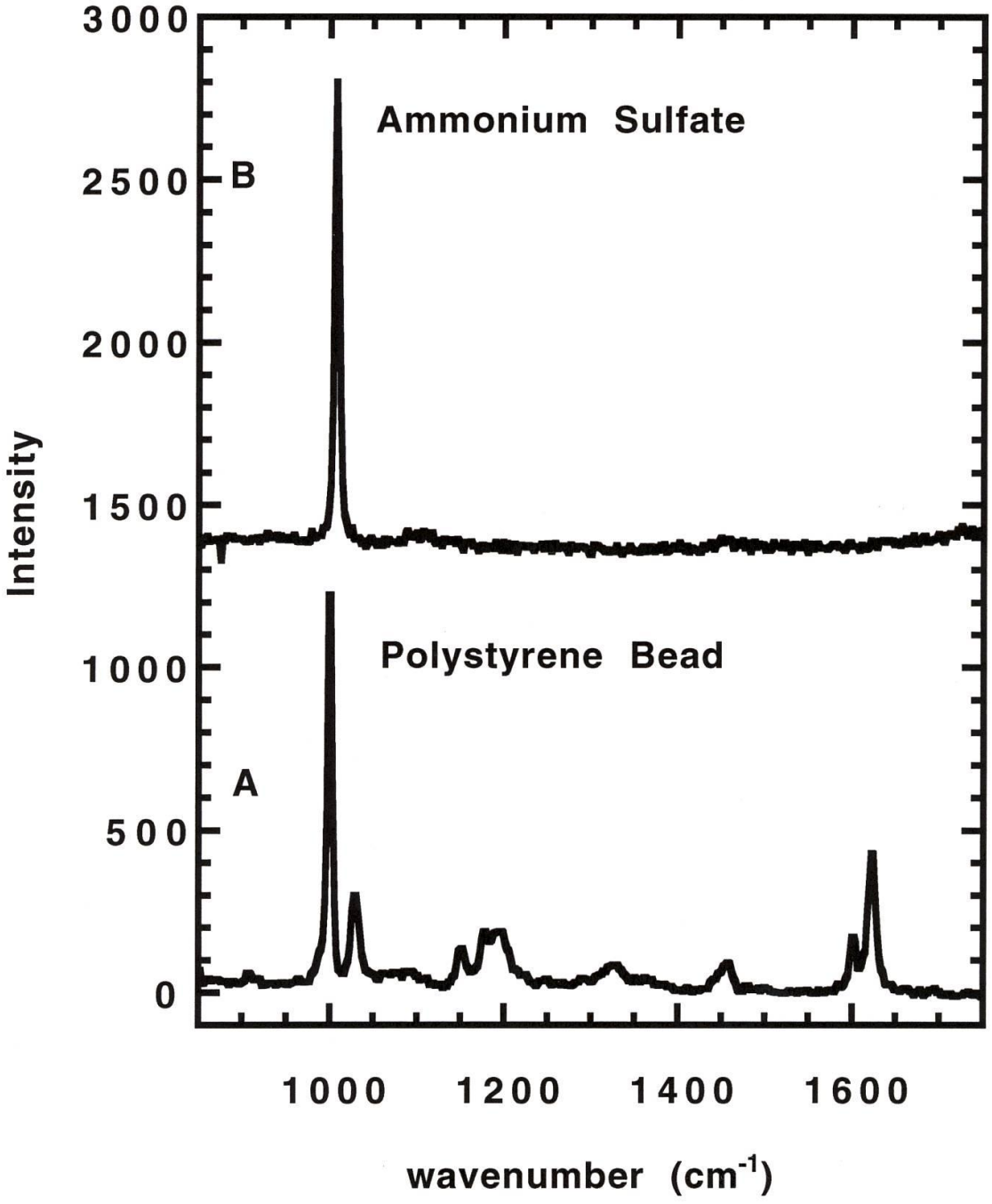

Figure 2, Hastings and Dyer

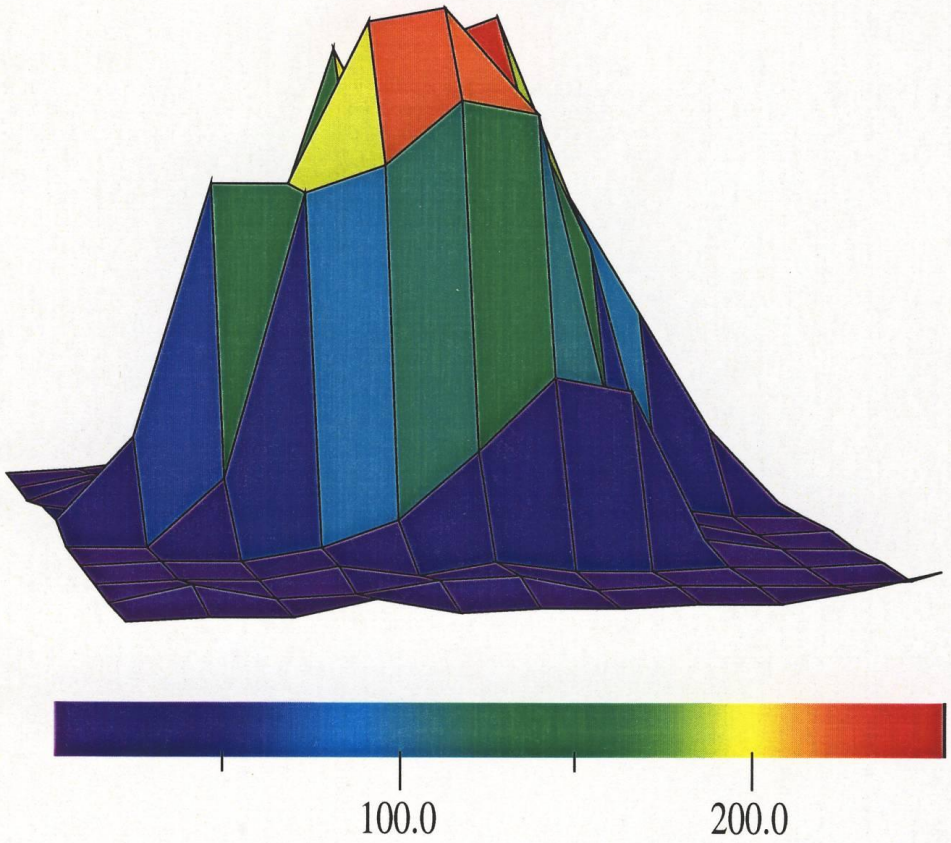

Figure 3, Hastings and Dyer

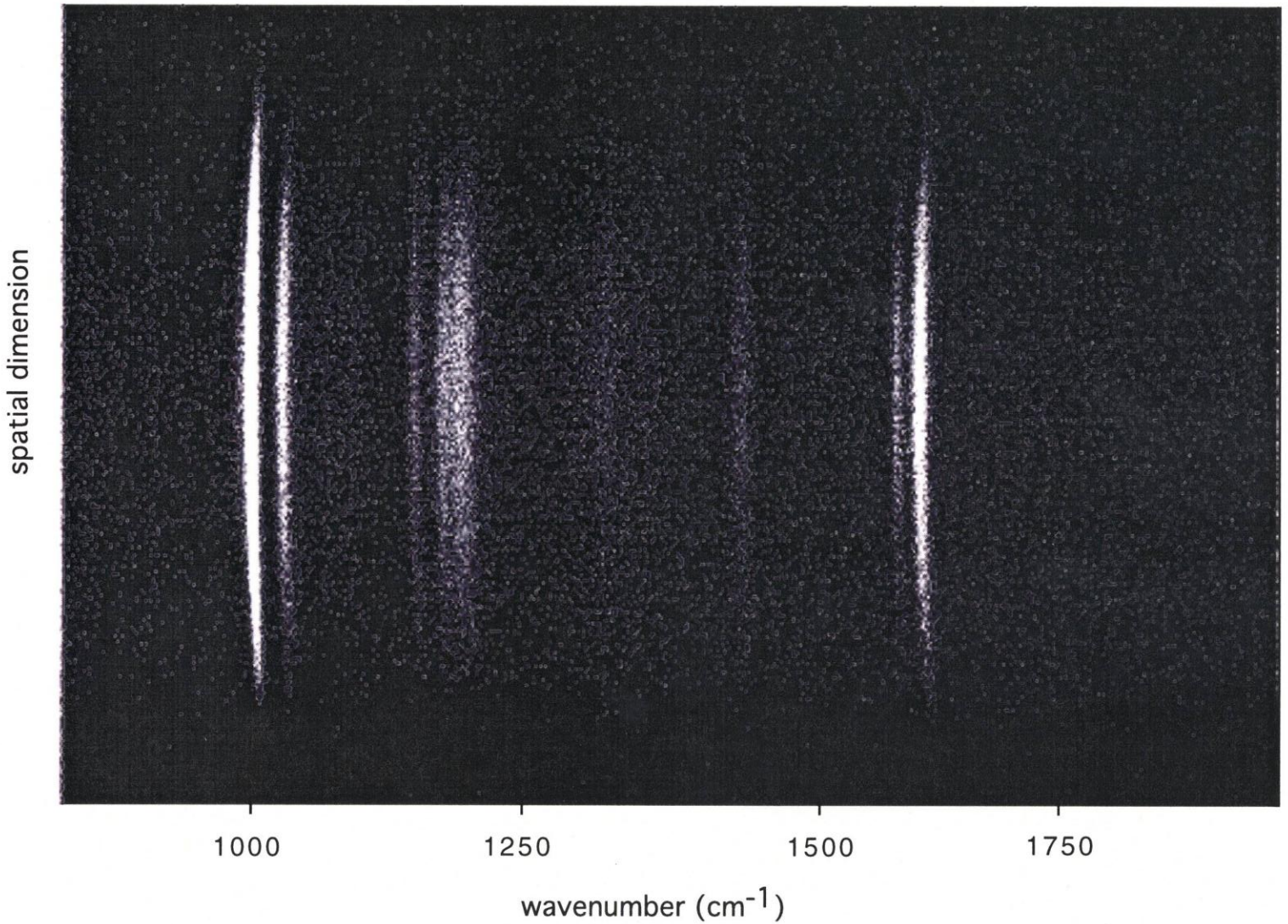

Figure 4, Hastings and Dyer

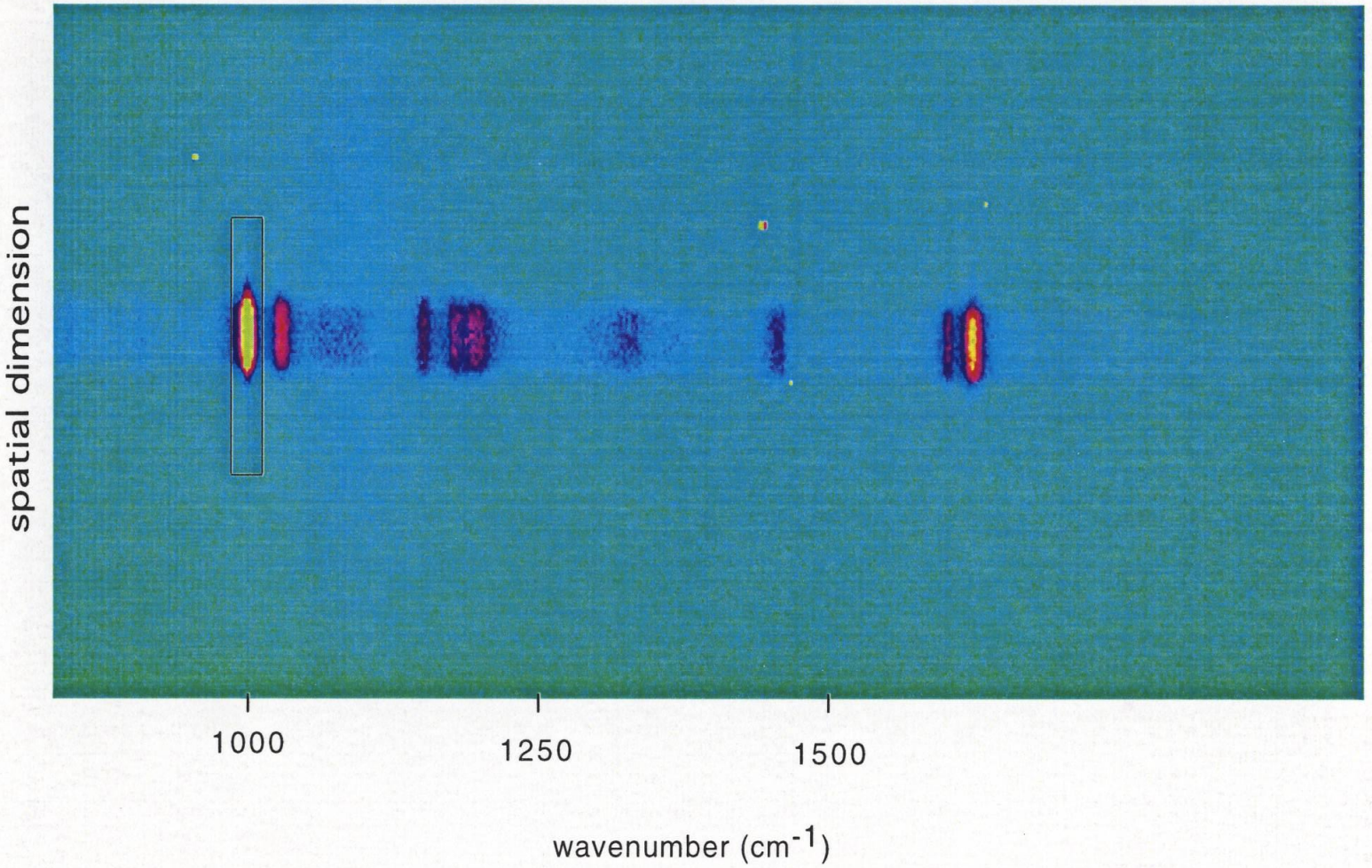

Figure 5, Hastings and Dyer

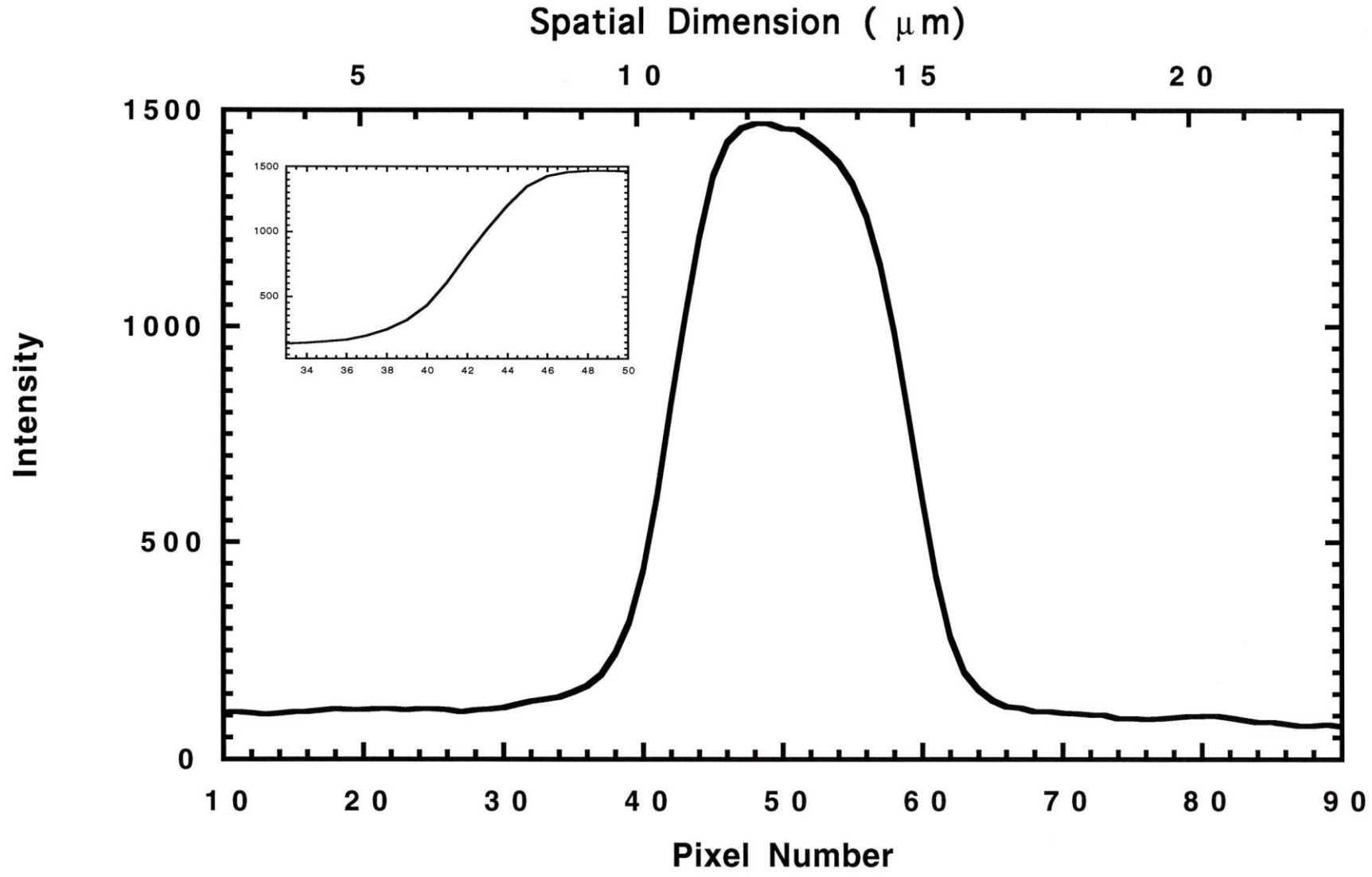

Figure 6, Hastings and Dyer

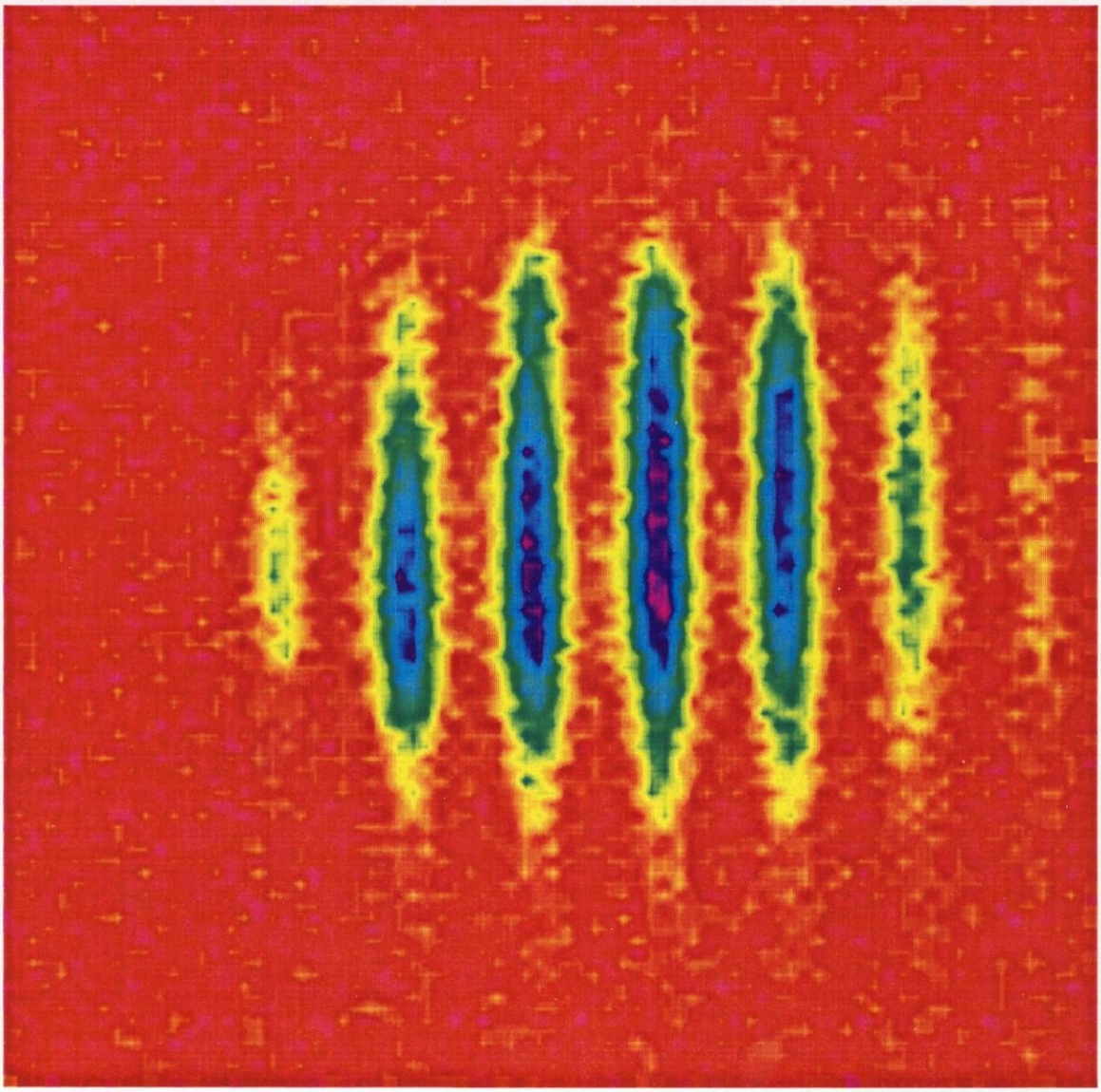

Figure 7, Hastings and Dyer

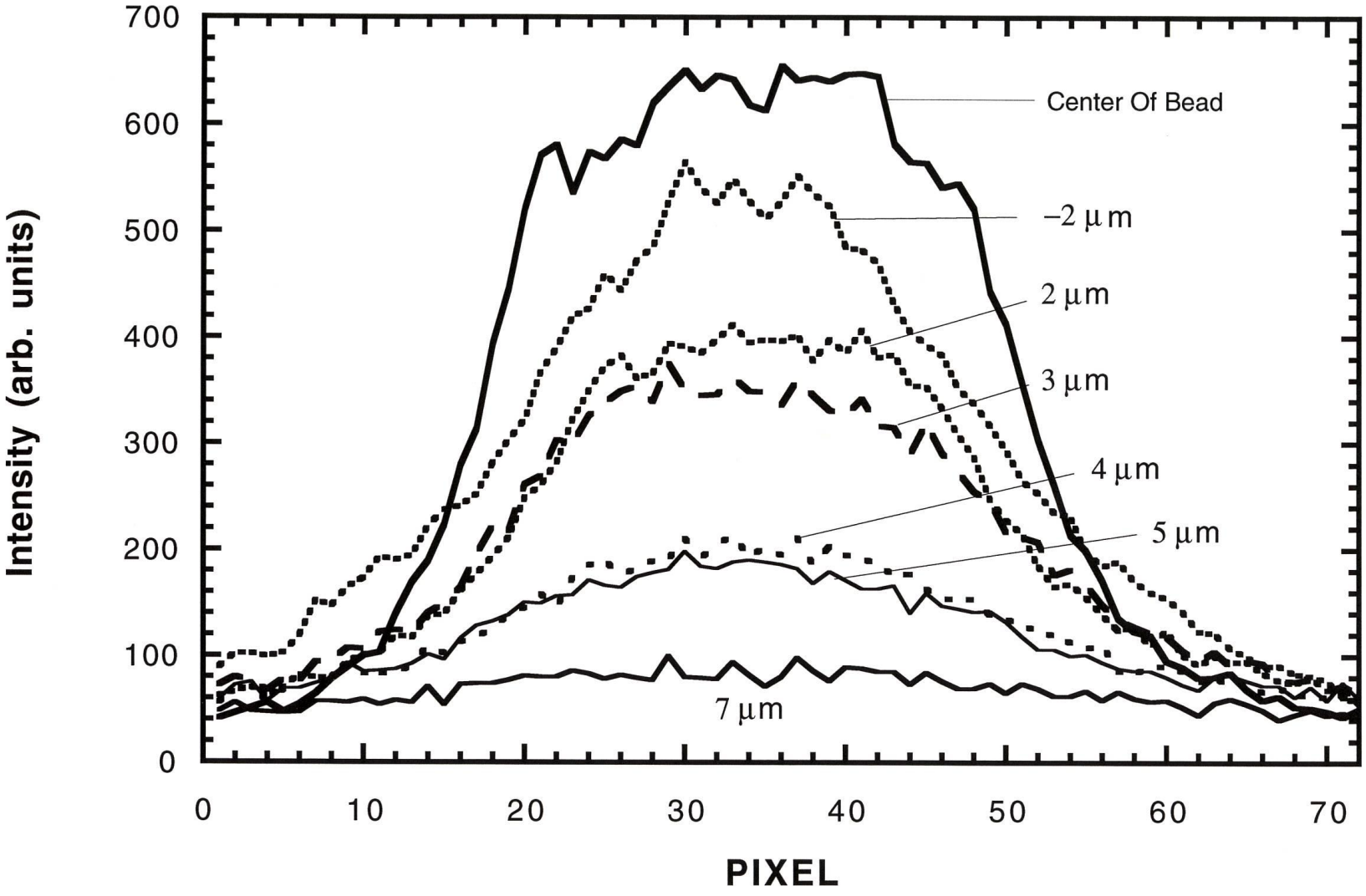

Fig. 8, Hastings and Dyer

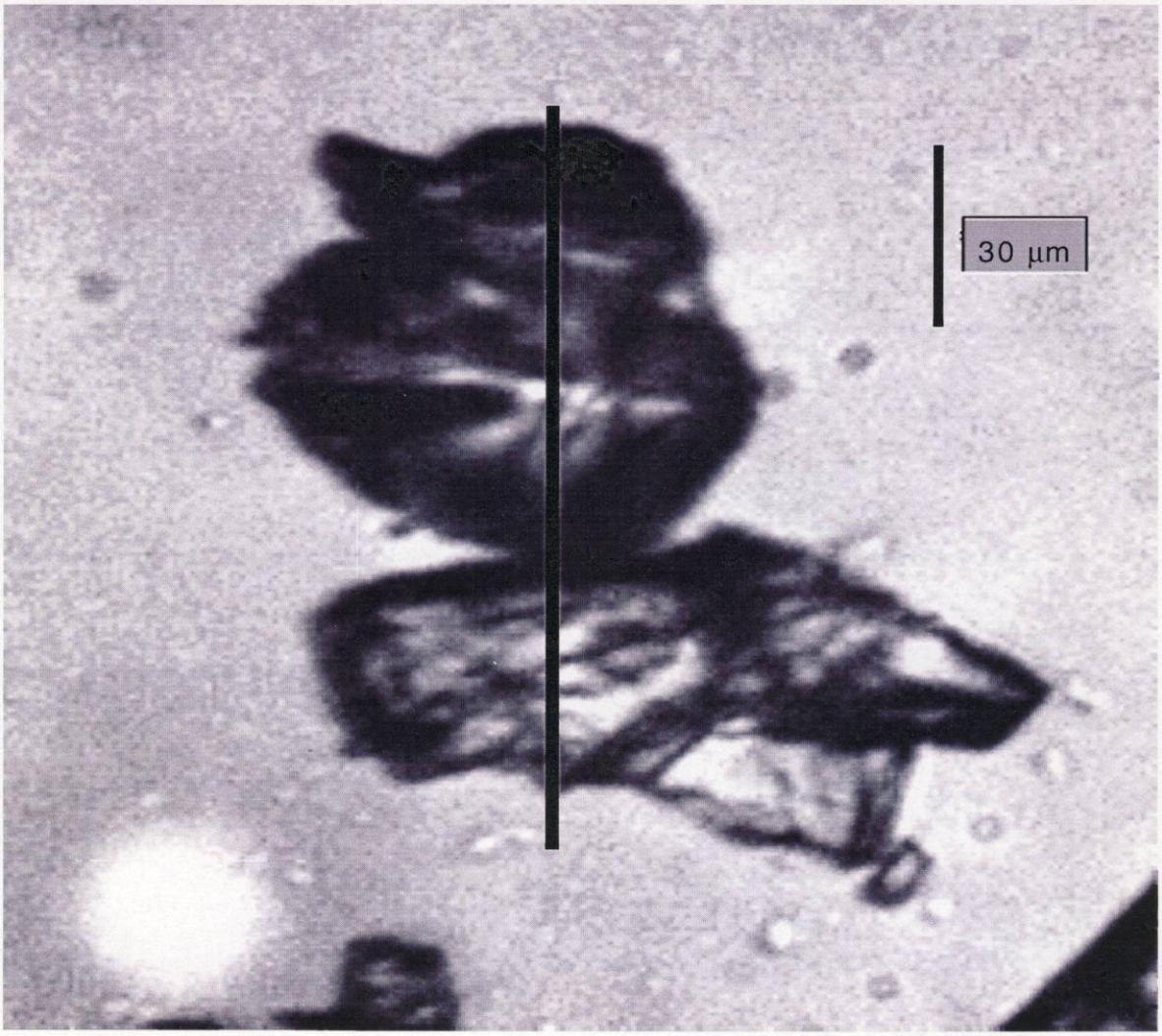

Figure 9, Hastings and Dyer

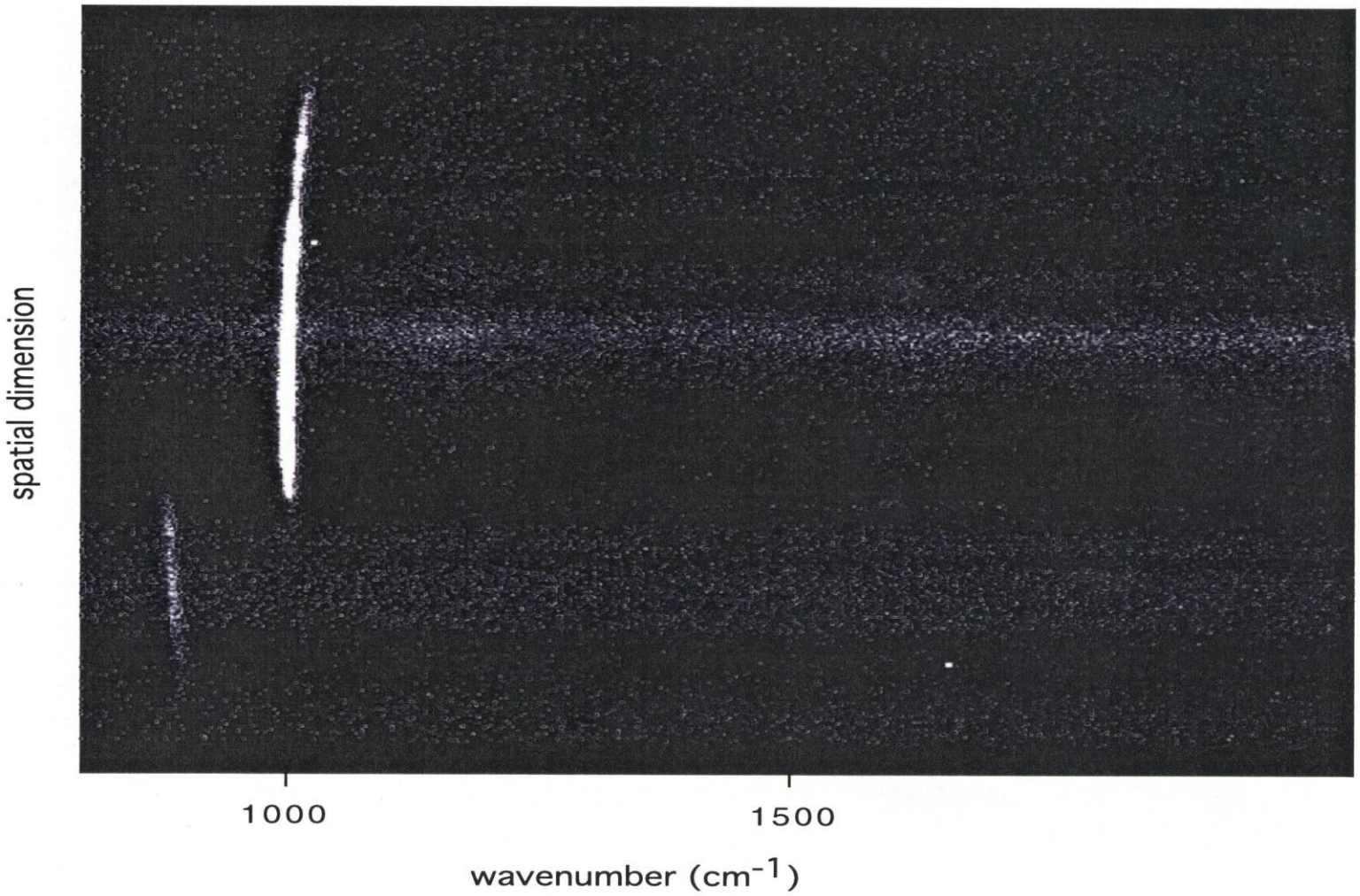

Figure 10, Hastings and Dyer

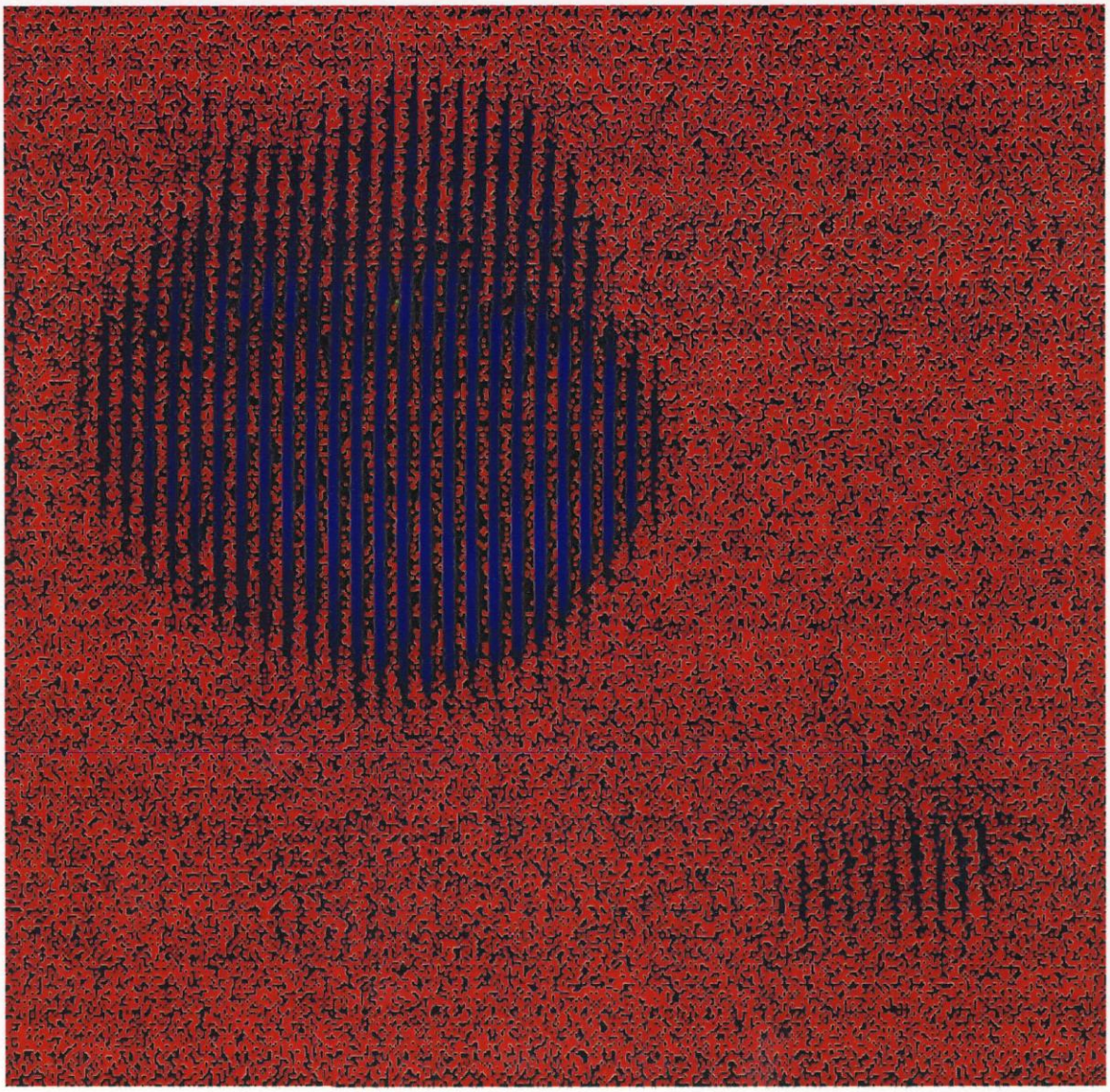

Figure 11, Hastings and Dyer

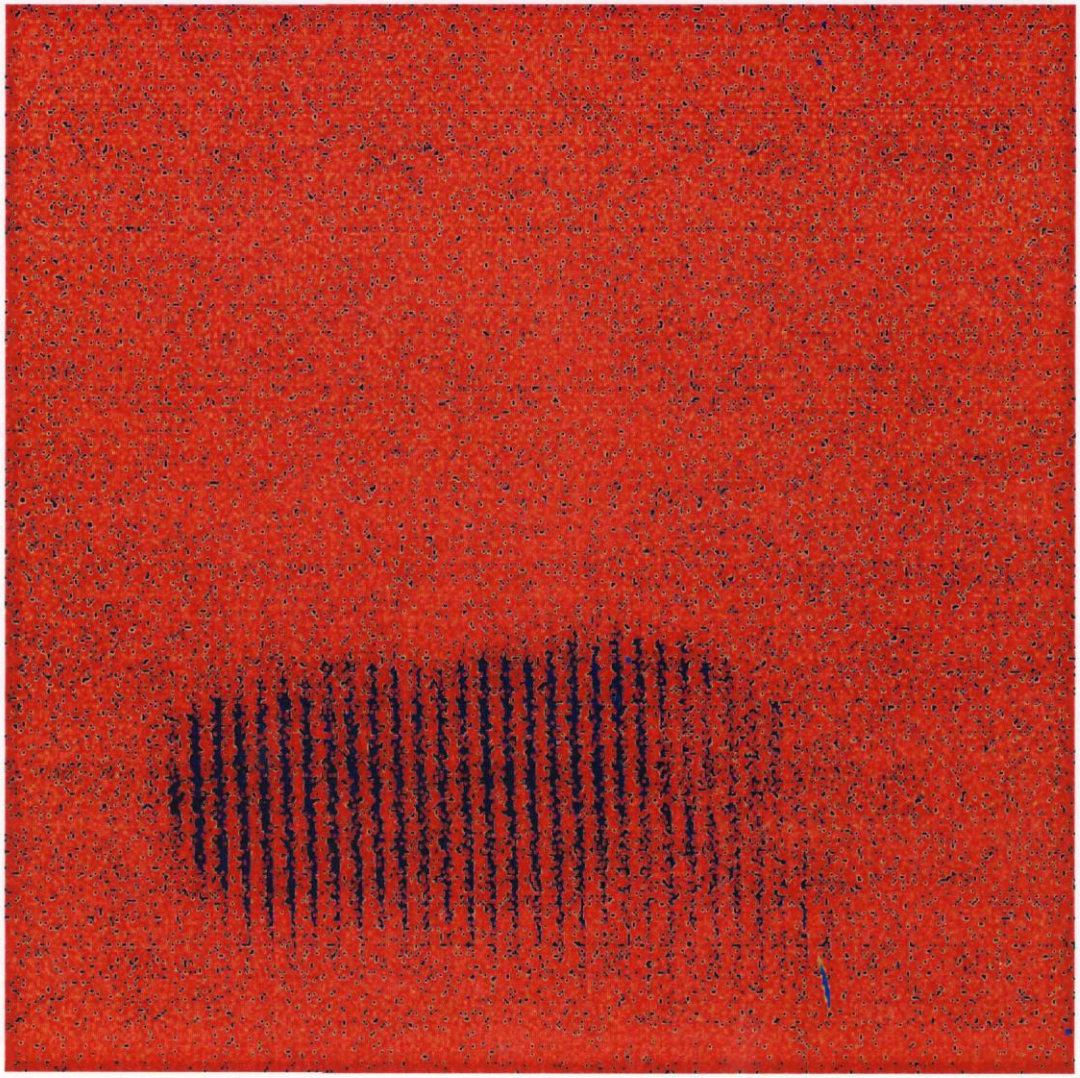

Figure 12, Hastings and Dyer

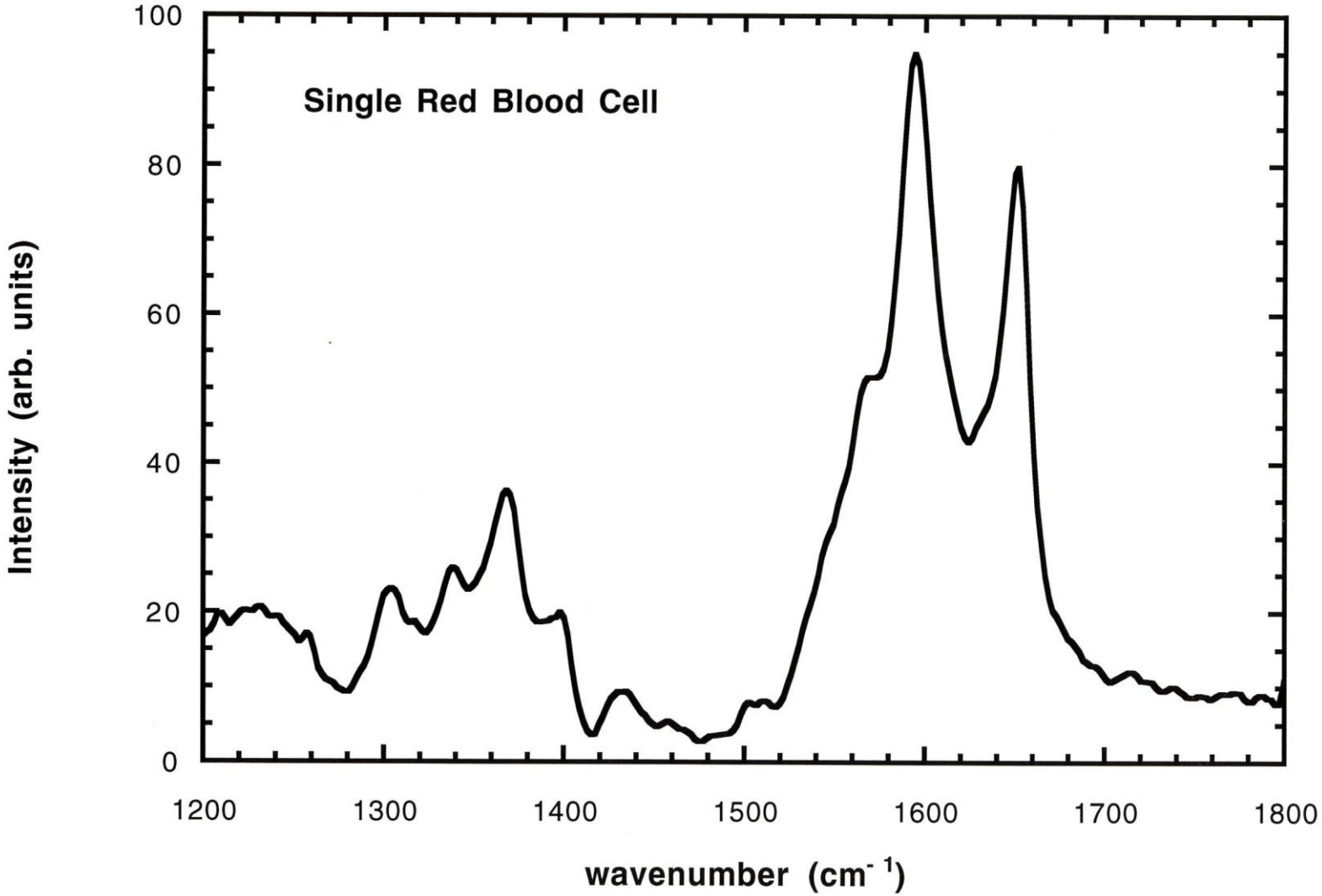

Figure 13, Hastings and Dyer

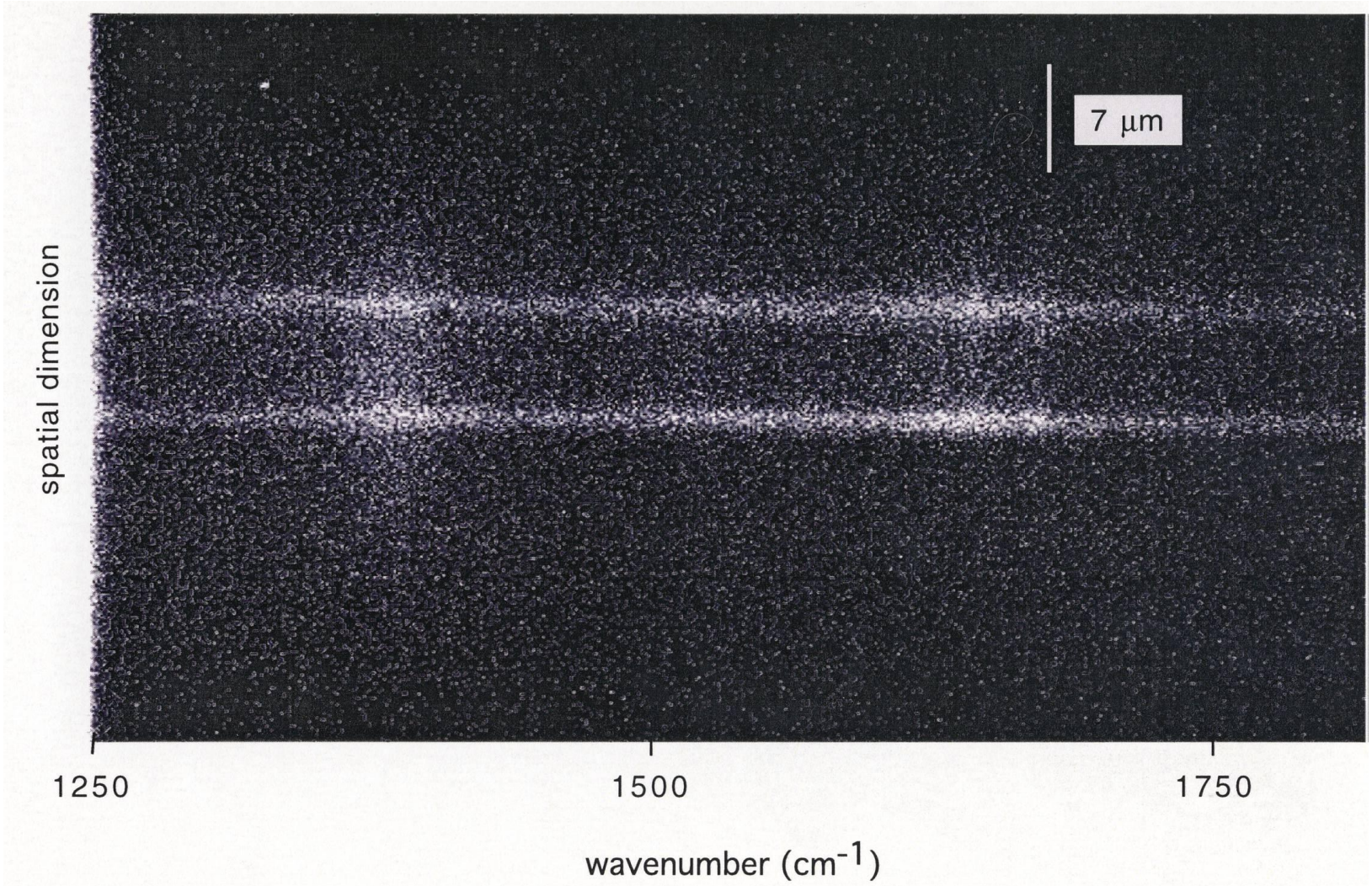

Figure 14, Hastings and Dyer